ICARUS 128, 75–82 (1997)
ARTICLE NO. IS975725

Dependence of Mercurian Atmospheric Column Abundance Estimations on Surface-Reflectance Modeling

Deborah L. Domingue

Lunar and Planetary Institute, 3600 Bay Area Boulevard, Houston, Texas 77058
E-mail: domingue@lpi.jsc.nasa.gov

and

Ann L. Sprague and Donald M. Hunten

University of Arizona, Lunar and Planetary Laboratory, Tucson, Arizona 85721

Received June 24, 1996; revised December 2, 1996

Column abundance estimates of sodium, and analogously, potassium, in Mercury's exosphere are strongly correlated to the surface reflection model used to calibrate the spectral data and the surface reflection model incorporated into the atmospheric radiative transfer solution. Depending on the surface reflection model parameters used, there can be differences in calibration factors of up to ±30% and differences in estimated column abundance of up to ±35%. Although the surface reflectance may not be used in the calibration of spacecraft measurements, the interaction between the reflected surface light and the atmospheric brightness remains important. © 1997 Academic Press

INTRODUCTION

The sources and sinks of Mercury's atmospheric sodium and potassium are not well known. Efforts to understand them better require knowledge of the distribution of Na and K about the planet. Linking spatial variations in column abundances to potential sources and sinks would increase our knowledge of Mercury's surface and atmospheric chemistry. This study examines the effect of chosen parameter values for the surface reflectance model on the calculation of mercurian atmospheric column abundances. We show that the reflectance properties of the mercurian surface can have significant effects on the abundances calculated from spectroscopic data. The results of this study define what level of column abundance spatial variability could be ascribed to current data reduction methods.

We assume that groundbased observations of spectral lines are calibrated with reference to the brightness of Mercury's surface at a nearby wavelength. The advantage of this procedure is that the calibration data are from the same exposure as the line data. They share all the sky conditions, such as clouds near the horizon. The disadvantage, one of the points emphasized in this paper, is that the brightness of the surface is somewhat uncertain. Calibration against a standard star may be preferable for observations from a spacecraft, but not from the ground.

Regardless of the methodology used for the calibration and column abundance determinations, the surface reflection theory used in the mercurian atmosphere literature is Hapke's model (Hapke 1981, 1984, 1986). Our study focuses on the effects of the choice of Hapke model parameters on the calculated column abundances of Na in Mercury's atmosphere. Here we work with six Hapke parameter sets, each of which satisfies the disk integrated photometry of Danjon (1949) for Mercury. To accomplish our goal we have reduced and analyzed sodium emission measurements from January 23, 1988 (Sprague *et al.* 1996a), obtained at the Catalina Observatory outside Tucson, Arizona. The observations were made using the LPL échelle spectrograph, mounted in the focal plane of the 1.5-m telescope.

ROLE OF HAPKE'S MODEL

Hapke's model (Hapke 1981, 1984, 1986) is a function of incident, emission, and phase angles. The parameters include the single scattering albedo, w, the opposition effect parameters b_0 (amplitude) and h (width), the surface roughness parameter, θ, and the single particle scattering function (which may have one to three parameters). Table I and Figure 1 display six viable solution sets to the Hapke model parameters based on modeling Danjon's (1949) disk-integrated phase curve of Mercury. The first three Hapke model solutions listed use a two parameter Legendre polynomial of the form

$$p(\alpha) = 1 + b\cos(\alpha) + c(3\cos^2(\alpha) - 1)/2$$

0019-1035/97 $25.00

TABLE I
Hapke Parameter Solution Sets to Mercury's Disk-Integrated Phase Curve

Parameter	Set 1[a]	Set 2[a]	Set 3[a]	Set 4	Set 5	Set 6
w	0.21	0.20	0.23	0.22	0.218	0.286
bo	1.85	2.4	2.5	1.0	1.0	1.0
h	0.03	0.11	0.09	0.0604	0.0284	0.0438
b	0.40	0.20	0.18	0.268	0.266	0.307
c	0.40	0.18	0.15	0.276	0.148	0.531
θ-bar	20	21	25	22	20	32
rms	0.121	0.162	0.212	0.118	0.124	0.117

[a] Used a Legendre polynomial for the single particle scattering function. Others used a double Henyey–Greenstein function. Error bars: $w = \pm 0.02$, bo $= \pm 0.02$, $h = \pm 0.01$, $b = \pm 0.05$, $c = \pm 0.05$, θ-bar $= \pm 5$. rms is the root mean square difference between the data and the model. It is defined as the square root of the sum of: the differences squared divided by the number of data points.

for the single scattering function, where α is the phase angle. The first solution is taken from Bowell *et al.* (1989) and the second and third solutions are solutions 1 and 2 from Veverka *et al.* (1988). The last three Hapke model solutions use a two parameter double Henyey–Greenstein function of the form

$$p(\alpha) = \frac{(1-c)(1-b^2)}{(1-2b\cos(\alpha)+b^2)^{3/2}} + \frac{c(1-b^2)}{(1+2b\cos(\alpha)+b^2)^{3/2}}$$

for the single scattering function, where α is the phase angle. These solutions were found using a modified least squares grid search and are published here for the first time.

Surface reflection modeling enters into the calculation of sodium and potassium column abundances in two ways: (1) in determining the instrument sensitivity and (2) in calculating the emission from atoms induced by the absorbtion of reflected light from the surface. Absolute calibration assigns a value of brightness in rayleighs to the data numbers measured by the imaging device. The method of absolute calibration for atmospheric emissions from Mercury's atmosphere is reviewed in the next section; however, the details are available in Sprague *et al.* (1996b).

Calculations of column abundances must include resonant scattering induced by surface reflected light. Two dif-

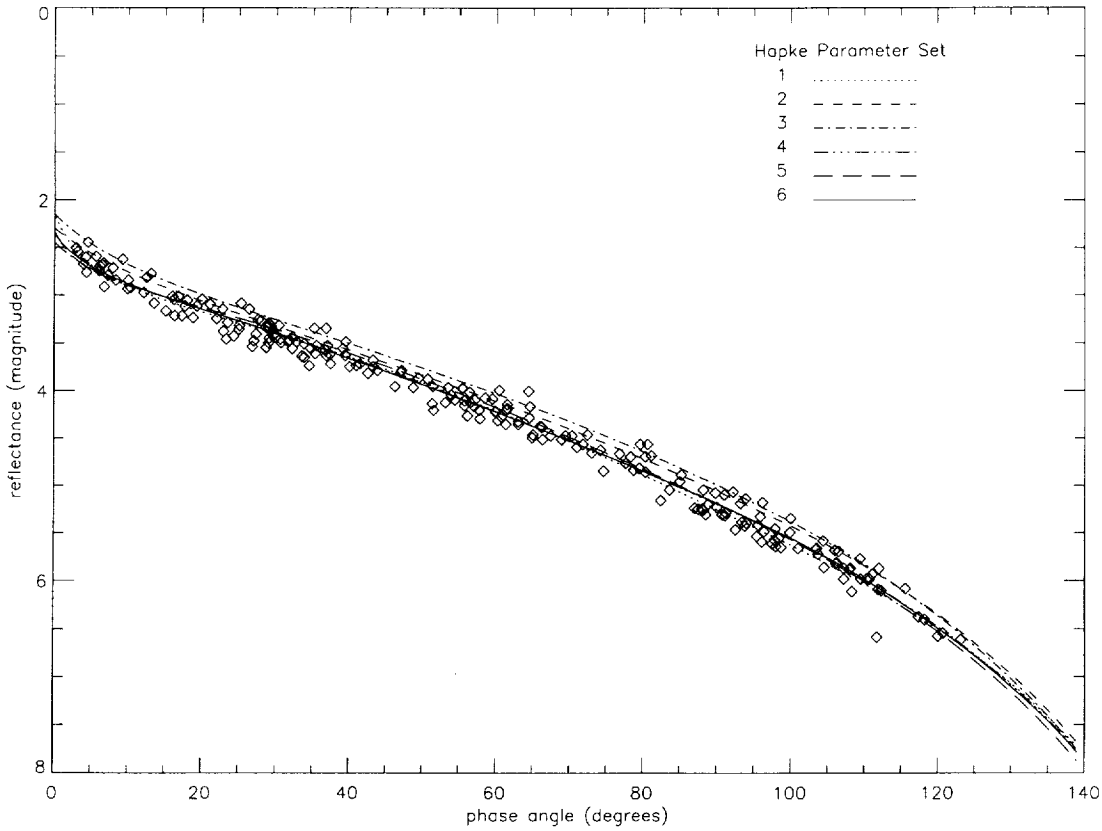

FIG. 1. Disk-integrated solar phase curve for Mercury. The open diamonds are Danjon's (1949) V filter observations of Mercury. The values of the parameter solution sets are listed in Table I.

TABLE II
Observing Parameters

Date UT	23 January 1988
Frame No.	168
UT start time	21 hr 10 min
Exposure time	50 sec
Mercury–Sun distance	0.3239273 AU
Phase angle	70.8°
Diameter	6.45 arcsec
Sub-Earth longitude	70.6°
Subsolar longitude	0.0°
Mercury–Sun doppler shift	−141 mÅ
Solar flux at Mercury	4.965×10^{14} quanta/cm^2 sec Å
g-factors (D2, D1)	36, 20 sec^{-1}

ferent approaches have been used to calculate the radiative transfer of sodium emission at Mercury. Killen (1988) and Killen *et al.* (1990) have used Chandrasekhar's solution to the planetary problem in terms of X and Y functions and their moments. The monochromatic results are then integrated over the lineshape. Hunten and Wallace (1993) adopted a doubling-adding numerical method with the approximation of complete frequency redistribution (CFR). Though the results of the two methods have not been compared, both should have ample accuracy. Both models assume a Maxwell–Boltzmann distribution for the velocity, which may not be the case for Mercury's atmosphere. However, for this study we are concerned only with uncertainties related to the surface reflection model.

ALGORITHM FOR TESTING DATA REDUCTION METHOD

Using an actual spectrum showing Na emission along a north–south (N/S) slit across Mercury's Earth-facing disk (Sprague *et al.* 1996a), we calculated the column abundances six times, once for every set of Hapke model parameter solutions given in the previous section. The goal was to examine any changes in the estimated column abundances owing to the choice of Hapke parameters.

The Atmospheric Sodium Emission Data

Table II gives the physical parameters of Mercury for the atmospheric measurements considered here. For this particular observation the spectrograph slit was placed across the illuminated sector, in the N/S direction, of a gibbous planet (70.8° phase angle) and offset from the central meridian by ~2 arcsec or ~0.6 mercurian radii. The N/S data scan is divided into five sectors which are correlated with a physical position (latitude and longitude) by using an appropriate model which includes the effects of seeing smear (σ). The seeing σ is defined as the half width at the $1/e$ point of a two-dimensional gaussian. Estimations of the seeing smear were made by generating a model of the surface reflectance and smearing it to a variety of seeing σ. The seeing σ for the data is determined by comparing a N/S scan from each version of the smeared model to the actual planetary data within the continuum portion of the spectrum and finding the scan from the smeared models which most closely approximates the shape and relative size dimensions of the continuum scan from the data. Table III lists the σ values calculated using each of the Hapke model parameter solution sets to generate the initial surface reflectance model.

The instrument sensitivity or calibration factor (CF = brightness giving 1 DN/sec) is given by

$$\mathrm{CF} = B_S/Q \text{ krayleigh sec DN}^{-1},$$

where B_S is the surface brightness and Q is defined as the average number of data counts (DN) per angstrom per second. The surface brightness (B_S) is given by

$$B_S = F_\lambda \times 4\pi R_R \cdot 10^{-12} \text{ Mrayleigh Å1}^{-1},$$

where F_λ is the solar flux at Mercury at wavelength λ and R_R is the average surface reflectance from the center of a swath across the smeared model corresponding to the slit across Mercury from which the data were taken. The values for B_S, Q, and CF are listed in Table III as derived from each of the six Hapke model parameter solution sets.

Column Abundance Calculations

Column abundances were calculated using the method of Hunten and Wallace (1993) which accounts for the self-shadowing of sodium radiation by its own column of atoms above the surface. Calculations of the sodium column abundances were made using this method for each of the Hapke model parameter solution sets with the corresponding seeing σ and calibration factors. The contribution of sodium emission due to the resonant scattering induced by the absorbtion of surface reflected light depends directly

TABLE III
Data Reduction Parameters

Solution set Nos.	σ	B_S	Q	CF
1	1.74	48.6	279.09	174.1
2	1.79	54.3	279.09	194.5
3	1.81	59.4	279.09	212.8
4	1.79	54.7	279.09	196.2
5	1.74	54.7	279.09	196.2
6	2.00	31.8	279.09	113.9

Note. B_S is in Mrayleighs Å^{-1}; Q is in DN Å^{-1}sec^{-1}; CF is in krayleigh sec DN^{-1}.

upon the calculated surface reflectance values (R_R) based on Hapke's model. In order to separate the Hapke model's influence on the calibration factor and seeing σ from its influence on the atmospheric scattering functions and the interpolation and self-shadowing process, we did two different numerical experiments. First we generated six self-consistent models in which the seeing σ's, calibration factors, and suites of column abundances are calculated from the same Hapke model parameter values. Second, we used the same calibration factor and seeing σ (the average of the values listed in Table III) for each of six trial runs that utilized only the unique atmospheric scattering function corresponding to the specific Hapke model parameter set in the interpolation.

RESULTS

Table III and Figs. 2 and 3 summarize our results. The self-consistent trials produced different column abundances as shown in Fig. 2. Differences of up to ±7% are found for the seeing σ calculations and differences of up to ±27% are found for the calibration factors. The end result is differences of up to ±35% in the estimated column abundances. Figure 3 shows the results of the second numerical experiment, where the same values of the seeing σ and the calibration factors (1.8 arcsec and 181 krayleigh sec DN^{-1}, respectively) were used. The results show that the choice of parameters used in the Hapke model affect the radiative transfer solution up to ±9%, considerably less than in the first case. The greatest effect of the Hapke model is in the data calibration.

All of these calculations assume an optically thick atmosphere. An analogy can be made for an optically thin atmosphere (as is the case for potassium). The calculations for the calibration factor and seeing smear are the same for both types of atmosphere; therefore, variations in their values due to Hapke parameter values are the same. However, the self-shadowing effects are much different. In the optically thin case the self-shadowing effects are linear; therefore, variations in column abundance estimates due to absorbtion by the atmosphere of surface reflected light are directly proportional to the variations in the modeled surface reflectance values (R_R). In the optically thick case the self-shadowing effects are highly non-linear, and therefore have been calculated.

DISCUSSION

Calculations of the magnitude of the effect of different choices of Hapke model parameters on the estimated properties of Mercury's exosphere show that the larger effect is in the deduced calibration factor. This will change the estimated intensities for the whole observation. A second, smaller, effect occurs due to different estimates of the amount of illumination of the atmosphere by surface reflected radiation.

Hapke model solutions to a disk-integrated phase curve are descriptive of the reflectance properties of the average surface. If the assumption is made that the surface of Mercury is homogeneous, then the solution to the disk-integrated phase curve should provide a reasonably accurate description of any subarea on Mercury. Note, however, that all six parameter solution sets in Table I are from viable fits of Hapke's model to Mercury's disk-integrated phase curve. Depending on which of these parameter sets is incorporated into the surface reflection model, the column abundances may be over- or underestimated by up to ±35%. In addition, while any variations seen in the column abundances as a function of position on the disk are real, the magnitude of these variations will also be strongly dependent on the choice of parameters used in the surface reflection model. If, however, Mercury's surface is heterogeneous, then the surface reflectance for different areas on Mercury are described by different Hapke model parameter sets. If this assumption is valid, the calibration factor derived for a data set will correspond to a mean reflectance for the entire area near the center of the image. This reflectance will probably be reasonably well described by one of the disk-integrated parameter sets, and the error in the calibration factor will be as previously discussed. The illumination of the atmosphere by light from the surface will, however, not be correctly described, and errors of up to 5% might be made in the deduced abundance as illustrated in Fig. 3. These 5% spatial uncertainties may be a lower limit. Murray *et al.* (1974) found that the brightness variations across Mercury's surface from Mariner 10 data are similar to those seen for the Moon, and they estimated normal albedos (measured at 5° phase) to range from 0.09 to 0.45 (Veverka *et al.* 1988). While 5% uncertainties are probably well within the noise of groundbased observations, they may be significant for future spacecraft observations.

If Mercury's surface is heterogeneous, then the only valid method for determining the surface reflectance properties is to model disk-resolved data of the surface. Disk-resolved data do not currently exist at the number of viewing geometries needed to adequately constrain the values of the Hapke model parameters. Because of seeing smear, light along the observing slit in the continuum portion of the groundbased spectra does not display spatial variations in brightness. Thus the assumption of a homogeneous surface on Mercury is a valid first approximation considering the spatial resolution of the atmospheric data. This will not be true for future spacecraft observations, as demonstrated by the normal albedo variations seen by Mariner 10 (Murray *et al.* 1974, Veverka *et al.* 1988).

With respect to groundbased observations, we ask which, if any, of the Hapke model parameter solution sets pre-

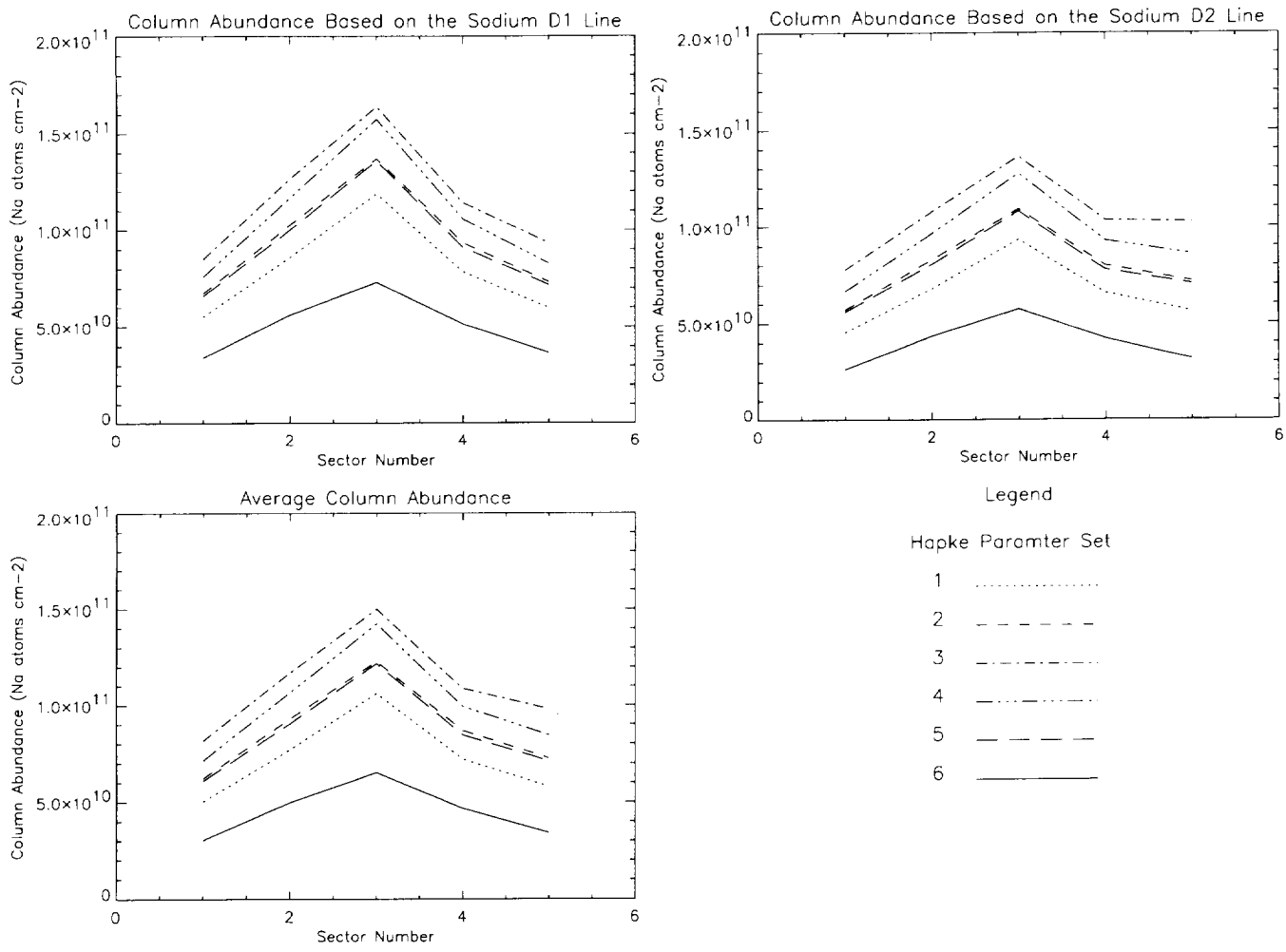

FIG. 2. The sodium column abundances along a north–south slit of Mercury corresponding to an observation along the illuminated hemisphere of a 70.2° solar phase observation. The values of the parameter solution sets are listed in Table I.

sented here is the most reasonable choice for describing Mercury's surface. This may greatly influence the column abundance calculated from the spectroscopic observations. One method of determining if one set of disk-integrated parameters is a better description of the surface than another is to compare the fits of each of the parameter solution sets to disk-resolved data. Figure 4 shows two scans across the disk of Mercury taken from an orange filter Mariner 10 image digitized from similar plots shown by Bowell *et al.* (1989). The Mariner 10 orange filter has an effective wavelength of 575 nm (Hapke *et al.* 1975) compared to the 550-nm effective wavelength of Danjon's (1949) *V* filter data. Accounting for the differences in wavelength and the fact that the spacecraft disk-resolved data and the groundbased disk-integrated data were taken by two different instruments under extremely different observing conditions, Fig. 4 shows that all of the parameter solution sets listed in Table I, with the exceptions of sets 1 and 6, are reasonable fits to the Mariner 10 disk-resolved data. The best fits are given by parameter sets 2 and 3 (also known as solutions 1 and 2 from Veverka *et al.* (1988)). Note that the column abundance estimates between the Hapke parameter solution sets 2 and 3 vary by approximately ±10%.

Another consideration is the relationship between the parameter values and the physical attributes they describe. For example, Hapke's model assumes that the opposition effect is due entirely to shadow-hiding. Therefore b_0 is defined as the fraction of $wp(\alpha)$ that is scattered from the portion of the particle surface facing the source (Domingue and Hapke, 1989). By its physical definition the opposition amplitude parameter, b_0, should not exceed unity. However, Hapke (1990) and Mischenko (1992) have recently shown that an additional method for producing the opposi-

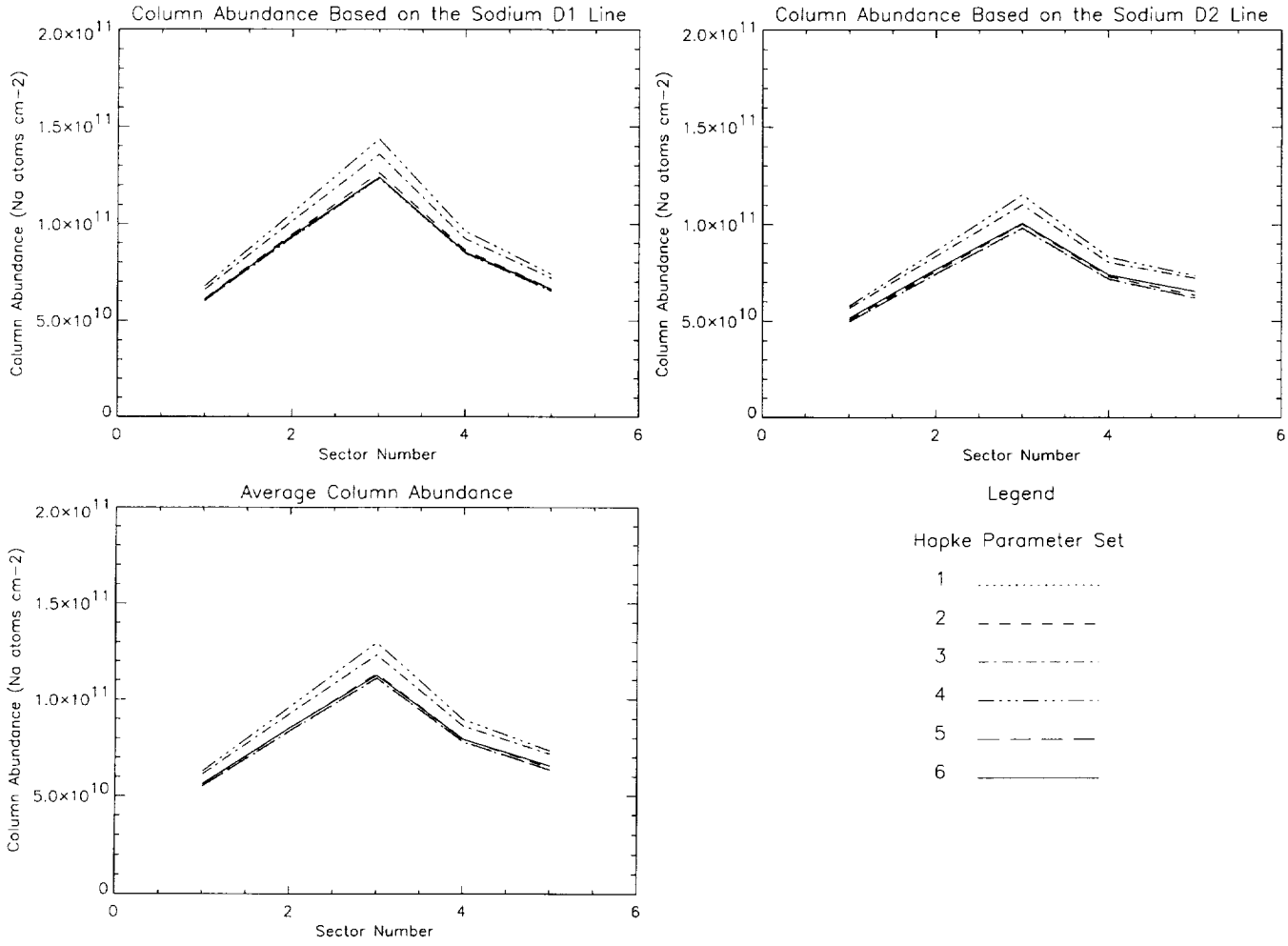

FIG. 3. The sodium column abundances along a north–south slit of Mercury corresponding to an observation along the illuminated hemisphere of a 70.2° solar phase observation. The values of the parameter solution sets are listed in Table I. Unlike the column abundances plotted in Fig. 2, these abundances assume the same seeing σ and calibration factor for all estimates of the column abundance.

tion effect is coherent backscatter. Hapke *et al.* (1996) have shown, through reflectance and polarization studies of several lunar soil samples, that the opposition effect on the Moon is caused by a combination of shadow-hiding and coherent backscatter. Coherent backscatter may also produce a portion of Mercury's opposition effect. Values of b_0 greater than unity may result from this dual opposition effect mechanism.

SUMMARY

The Hapke parameter values chosen to model the surface roughness of Mercury (or by analogy, the Moon) affect the calibration factor, the estimate of the seeing σ, and the calculated column abundance. If a large data set is analyzed entirely with one parameter set under the assumption that the surface is relatively homogeneous, then relative abundances will not be affected. However, for abundances calculated over heterogeneous terrain that is not well-described by a single parameter set, relative abundances will be either under or overestimated. Some conditions are not suited to the exclusive use of one parameter set. For example, if a large, smooth, dark basin is embedded in a region with large-scale roughness and high albedo, the same Hapke parameter set cannot describe the entire region. This can result in up to ±35% uncertainties in column abundances, mostly through uncertainty in the calibration factor. Calibration for groundbased observations assume that the mercurian surface is of homogeneous roughness in the visible and near infrared wavelengths and can be described by one set of Hapke parameters. We do not have the necessary data to know if this assumption is

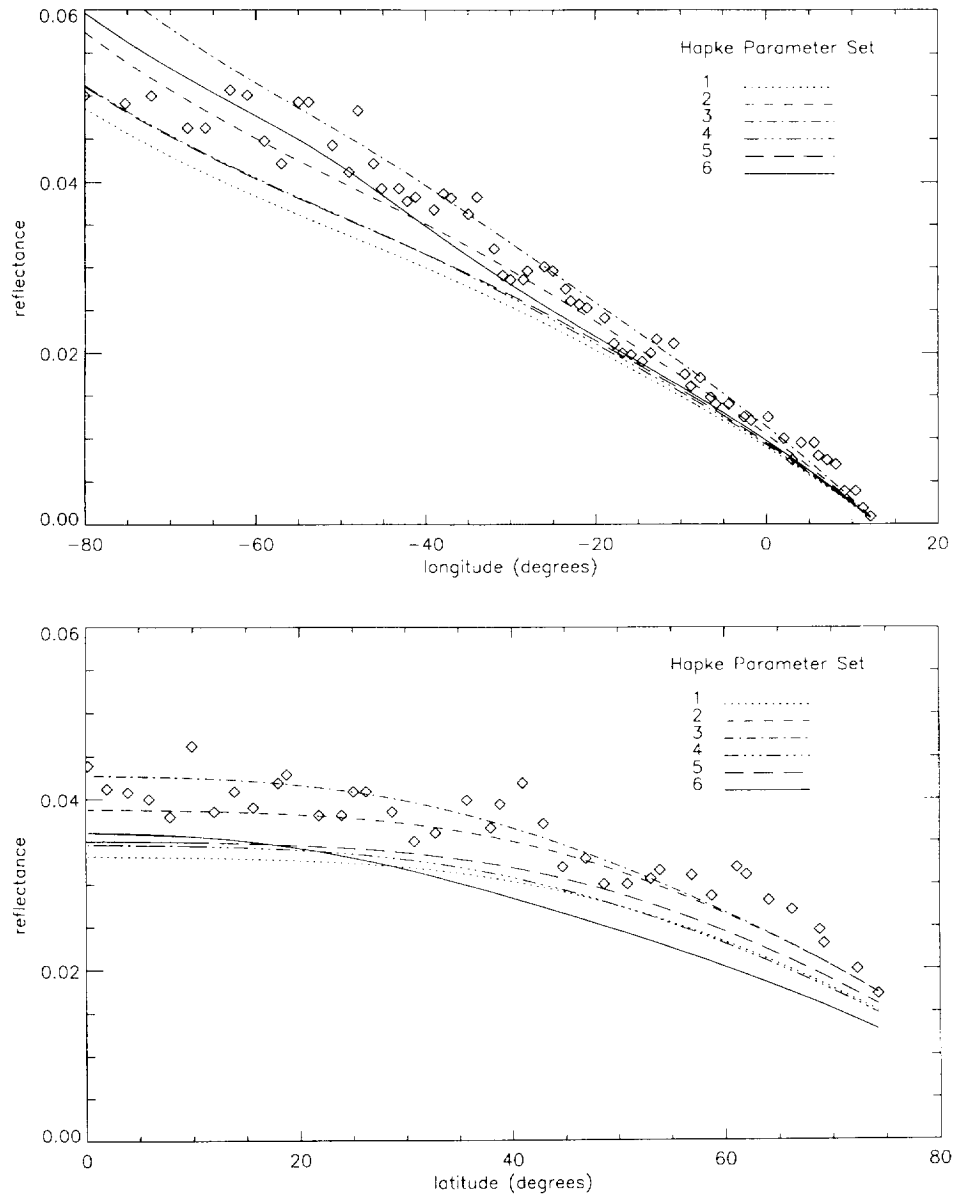

FIG. 4. Disk-resolved brightness curves along the photometric equator (top) and photometric meridian latitude of −50° (bottom) of an orange filter Mariner 10 image. The open diamonds represent the Mariner 10 data. The values of the parameter solution sets are listed in Table I.

valid for Na and K wavelengths; it certainly is not true in the centimeter wavelength range.

ACKNOWLEDGMENTS

The authors thank William Schmitt for his help in preparing the data for this project. They also thank Roger Yelle and Robert Nelson for helpful and insightful reviews. A. L. Sprague and D. M. Hunten were funded for this work by Grant NAGW-4308. LPI Contribution 917.

REFERENCES

Bowell, E., B. Hapke, D. Domingue, K. Lumme, J. Peltoniemi, and A. Harris 1989. Application of photometric models to asteroids. In *Asteroids II* (R. Binzel, T. Gehrels, and M. S. Matthews, Eds.), pp. 524–556. Univ. of Arizona Press, Tucson.

Danjon, A. 1949. Photometrie et Colorimetrie des Planetes Mercure et Venus. *Bull. Astron. (Paris)* **14,** 315–345.

Domingue, D., and B. Hapke. 1989. Fitting theoretical photometric functions to asteroid phase curves. *Icarus* **78,** 330–336.

Hapke, B. 1981. Bidirectional reflectance spectroscopy. I. Theory. *J. Geophys. Res.* **86,** 3039–3054.

Hapke, B. 1984. Bidirectional reflectance spectroscopy. 3. Correction for macroscopic roughness. *Icarus* **59,** 41–59.

Hapke, B. 1986. Bidirectional reflectance spectroscopy. 4. The extinction coefficient and the opposition effect. *Icarus* **67,** 3601–3618.

Hapke, B. 1990. Coherent backscatter and the radar characteristics of outer planet satellites. *Icarus* **88,** 407–417.

Hapke, B., G. E. Danielson, Jr., K. Klaasen, and L. Wilson 1975. Photometric observations of Mercury from Mariner 10. *J. Geophys. Res.* **80,** 2431–2443.

Hapke, B., R. M. Nelson, and W. D. Smythe 1996. The lunar opposition effect revisited. *Bull. Am. Astron. Soc.* **28,** 1122.

Hunten, D. M., and L. V. Wallace 1993. Resonance scattering by mercurian sodium. *Astrophys. J.* **417,** 757–761.

Killen, R. M. 1988. Resonance scattering by sodium in Mercury's atmosphere I. The effect of phase and atmospheric smearing. *Geophys. Res. Lett.* **15**(1), 80–83. [Erratum: *Geophys. Res. Lett.* **15**(3), 283]

Killen, R. M., A. E. Potter, and T. H. Morgan 1990. Spatial distribution of sodium vapor in the atmosphere of Mercury. *Icarus* **85,** 145–167.

Mischenko, M. I. 1992. The angular width of the coherent back-scatter opposition effect: An application to icy outer planet satellites. *Astrophys. Space Sci.* **194,** 327–333.

Murray, B. C., M. J. S. Belton, G. E. Danielson, M. E. Davies, D. E. Gault, B. Hapke, B. O'Leary, R. G. Strom, V. Suomi, and N. Trask 1974. Mercury's surface: Preliminary description and interpretation from Mariner 10 pictures. *Science* **185,** 169–179.

Sprague, A. L., D. M. Hunten, W. Schmitt, and R. W. H. Kozlowski 1996a. *Sodium in Mercury's Atmosphere: 1985–1988 Observations.* COSPAR abstracts (Birmingham, England), p. 51.

Sprague, A. L., D. M. Hunten, and F. A. Grosse 1996b. Upper limit for lithium in Mercury's atmosphere. *Icarus* **124,** 345–349.

Veverka, J., P. Helfenstein, B. Hapke, and J. E. Gougan 1988. Photometry and polarimetry of Mercury. In *Mercury* (F. Vilas, C. Chapman, and M. S. Matthews, Eds.), pp. 37–58. Univ. of Arizona Press, Tucson.